Proc. NIPR Symp. Antarct. Geosci., **8**, 137-159, 1995

K/Ar AND $^{40}Ar/^{39}Ar$ MINERAL AGES ACROSS THE LÜTZOW-HOLM COMPLEX, EAST ANTARCTICA

Geoffrey L. FRASER and Ian McDOUGALL

Research School of Earth Sciences, Australian National University, Canberra, ACT 0200, Australia

Abstract: K/Ar and $^{40}Ar/^{39}Ar$ mineral ages are presented for a variety of rock types from several localities across the high-grade Lützow-Holm Complex of East Antarctica. Results indicate setting of the K/Ar isotopic system took place between ~500-450 Ma throughout this terrain. These ages represent the time of cooling and stabilization of the region following Pan African orogenic activity as recorded by U/Pb zircon ages. Despite the broad consistency of ages, the results also indicate a significant variation in timing and rate of cooling between localities within the terrain, with average cooling rates being greater in rocks which experienced higher peak metamorphic conditions.

1. Introduction

The Lützow-Holm Complex (LHC) is one of several high-grade metamorphic terrains which collectively make up the East Antarctic Shield. It spans the Prince Harald, Sôya, and Prince Olav Coasts, between longitudes 39° and 45°E. Metamorphic basement rocks are exposed in numerous, relatively small, ice-free areas along this coast, separated by glaciers and the continental ice-sheet. To the east of an inferred tectonic boundary lie the Rayner and Napier Complexes of Enderby Land, whereas to the southwest, across several hundred kilometres of continental ice, lie the mountains of the Yamato-Belgica Complex.

Previous work in the LHC has documented an apparently systematic increase in metamorphic grade from east to west (Fig. 1), ranging from upper amphibolite facies on the eastern Prince Olav Coast to high temperature granulite facies in the head of Lützow-Holm Bay, then decreasing further west (HIROI *et al.*, 1991). Despite the variation in peak grade across the complex, all rocks appear to have experienced a similar "clockwise" style of *P-T-t* history during which early formed kyanite is replaced by sillimanite at peak conditions followed by the development of symplectitic decompression textures (*e.g.*, KAWASAKI *et al.*, 1993).

SHIRAISHI *et al.* (1994) obtained U/Pb zircon ages of ~550 Ma from several samples of different metamorphic grade within the LHC and interpret these zircon ages as the time of granulite facies metamorphism, making the LHC the youngest orogenic belt yet recognised in the East Antarctic Shield. This ~550 Ma age correlates with metamorphic ages from the Highland Series of Sri Lanka (*e.g.*, KRÖNER and WILLIAMS, 1993; HÖLZL *et al.*, 1994) which was most likely contiguous with the LHC before the breakup of Gondwana (DALZIEL, 1991). This is also the time of widespread metamorphism in eastern

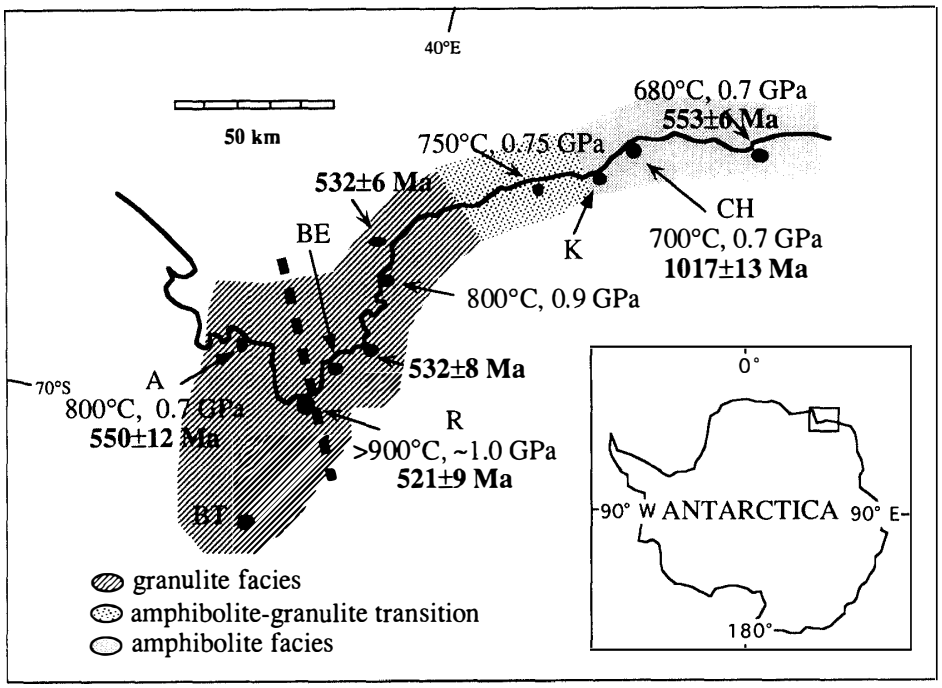

Fig. 1. Map of the Lützow-Holm Complex summarising the results of previous metamorphic and geochronological work. Estimates of peak metamorphic conditions are from MOTOYOSHI *(1993). Shading indicating metamorphic facies is after* HIROI *et al. (1991). The heavy dashed line is the thermal axis of* HIROI *et al. (1991). Ages given in bold are SHRIMP zircon ages from* SHIRAISHI *et al. (1994). Localities mentioned in the text are indicated by the following abbreviations; CH-Cape Hinode, K-Kasumi Rock, BE-Berrodden, R-Rundvågshetta, A-Austhovde, BT-Botnnuten.*

Africa, Madagascar and southern India (PAQUETTE *et al.*, 1994, and references therein), forming the Pan African Mozambique Belt, recording the collision of east Africa with India-Sri Lanka-Antarctica during the final amalgamation of Gondwana (DALZIEL, 1991).

In addition to the U-Pb zircon study of SHIRAISHI *et al.* (1994), several K/Ar and $^{40}Ar/^{39}Ar$ ages have been reported from Lützow-Holm Bay by KANEOKA *et al.* (1968), YANAI and UEDA (1974), SHIBATA *et al.* (1985) and TAKIGAMI *et al.* (1992). Most of the ages in these studies come from hornblende or biotite, and range between 363 Ma and 560 Ma.

Here we present K/Ar and $^{40}Ar/^{39}Ar$ mineral ages from several localities of different metamorphic grade in the LHC together with descriptions of the geological relations of the samples. Gneissic rocks in the Lützow-Holm Complex experienced peak temperatures ranging from ~650°C in the amphibolite grade area, to well over 800°C in the granulite facies zone. These temperatures are considerably higher than closure temperatures in the K/Ar system for commonly dated minerals. Consequently K/Ar dating of the gneissic rocks in the LHC is not expected to provide ages for peak metamorphic conditions, but should provide cooling ages which may be used to reconstruct the post-peak thermal history.

2. Analytical Techniques

Mineral separates of 99% purity were obtained by standard crushing, sieving, heavy liquid and magnetic separation methods. Hornblende separates generally required hand-picking to improve purity from ~95% to 99%.

Detailed technical descriptions of the K/Ar and $^{40}Ar/^{39}Ar$ techniques are given by DALRYMPLE and LANPHERE (1969) and MCDOUGALL and HARRISON (1988). For the K-Ar method, K analyses were via flame photometry after digesting the samples in H_2SO_4 and HF, and adding the resulting solution to a lithium sodium buffer. All K analyses were performed in duplicate with both results presented in Table 1. Argon extraction involved fusing a separate aliquot of sample in a Pyrex high vacuum line by radio induction heating. A spike of ^{38}Ar was added and the gas cleaned over CuO and Ti getters before isotopic analysis of the argon.

Samples for $^{40}Ar/^{39}Ar$ analysis were irradiated for 576 hours in the HIFAR reactor at Lucas Heights, New South Wales. Each sample was sealed within a circular aluminium container, with the appropriate flux monitor in another smaller container positioned centrally inside the sample container. For biotite samples the flux monitor was the biotite standard GA1550, with a K/Ar age of 97.9 ± 0.9 Ma, and for hornblende samples the hornblende standard 77-600 of K/Ar age 414.1 ± 3.9 Ma was used (MCDOUGALL and HARRISON, 1988). To reduce the production of neutron-induced ^{40}Ar a 0.2 mm thick cadmium liner was used to shield the samples from thermal neutrons. The sample container was inverted exactly half way through the irradiation period to reduce the effect of gradients in neutron flux across the container. After a period of cooling following irradiation, samples were step heated in a high vacuum line and the active gases removed before isotopic analysis of the argon in a VG 1200 gas source mass spectrometer. For each step in the heating schedule the sample was held at the specified temperature for 15 min. Data treatment was via the Macintosh software Noble. The following correction factors were used to account for K- and Ca-derived Ar isotopes;

$(^{36}Ar/^{37}Ar)Ca = 3.5 \times 10^{-4}$
$(^{39}Ar/^{37}Ar)Ca = 7.86 \times 10^{-4}$
$(^{40}Ar/^{39}Ar)K = 2.7 \times 10^{-2}$.

3. Results

Conventional K/Ar ages have been measured for biotite, hornblende, K-feldspar and one muscovite sample, from a variety of rock types from six localities in the LHC ranging in grade from upper amphibolite facies to the highest temperature granulites. Subsequent to the K/Ar analyses, eight of the samples were selected for $^{40}Ar/^{39}Ar$ step heating anaylses. Results are presented in Tables 1 and 2 and Figs. 2 and 3. Plateau ages quoted for the $^{40}Ar/^{39}Ar$ age spectra are step-size weighted means on the basis of the percent of ^{39}Ar in the contributing steps. Local field relations, descriptions of each of the samples, and a discussion of the ages are given below for each of the six areas sampled. Maps at 1: 25000 scale and explanatory notes are available for each area in the National Institute of Polar Research (Tokyo) Antarctic Geological Map Series.

Table 1. K/Ar data for the Lützow-Holm Complex from this study.

Field No.	ANU No.	Rock description	Mineral	K (wt%)	$^{40}Ar^*$ (10^{-10} mol/g)	$^{40}Ar^*/^{40}Ar$ (%)	Age (Ma)	Uncertainty (1σ)
K-12	93-515	biotite-hornblende gneiss	biotite	7.66, 7.62	75.05	65.7	492.4	5.1
K-12	93-515	biotite-hornblende gneiss	hornblende	0.941, 0.940	11.57	96.3	599.0	6.2
K-18	93-521	migmatitic segregation	biotite	6.69, 6.73	64.12	95.8	481.0	4.9
K-18	93-521	migmatitic segregation	K-feldspar	11.96, 11.90	109.29	95.5	463.3	4.7
K-30	93-533	migmatitic pegmatite	biotite	7.22, 7.21	67.57	97.2	472.4	4.8
K-34	93-536	leucocratic gneiss	biotite	7.15, 7.21	67.87	96.2	477.2	4.9
R-47	93-606	concordant pegmatite	biotite	7.88, 7.81	70.02	97.6	500.4	5.1
R-48	93-607	biotite gneiss	biotite	8.05, 7.99	83.09	98.5	516.1	5.3
R-60	93-617	late stage, linear pegmatite	biotite	7.14, 7.05	62.14	98.6	445.1	5.1
R-15	93-574	mafic dyke	hornblende	1.29, 1.28	13.22	92.6	512.4	5.6
CH-15	93-551	migmatitic pegmatite	biotite	8.12, 8.10	77.46	98.7	480.6	4.9
CH-17	93-553	discordant pegmatite	muscovite	8.62, 8.67	86.22	95.3	499.1	5.1
CH-4	93-540	amphibolite	hornblende	0.926, 0.90	9.73	95.6	526.2	5.4
A-23	93-675	gneissic granite	biotite	7.18, 7.13	63.32	83.6	449.3	4.6
A-34	93-695	garnet-pyroxene gneiss	hornblende	1.79, 1.78	18.00	96.6	502.0	5.3
BE-24	93-644	semi-concordant pegmatite	biotite	7.38, 7.39	69.73	95.3	475.7	5.3
BE-24	93-644	semi-concordant pegmatite	K-feldspar	11.70, 11.75	98.56	89.5	429.4	4.4
BT-1	93-1260	biotite-garnet gneiss	biotite	8.02, 8.06	75.24	90.1	474.0	4.9

Prefixes field numbers indicate the locality of the samples as follows; K = Kasumi Rock, R = Rundvågshetta, CH = Cape Hinode, A = Austhovde, BE = Berodden, BT = Botnnuten. Errors are quoted at the 1σ level, and arise from a combination of the errors in %K, $^{40}Ar^*$ and spike calibration. K/Ar ages should coincide with $^{40}Ar/^{39}Ar$ total fusion ages presented in Table 2, although the total fusion ages will be more precise. In some cases where both K/Ar and $^{40}Ar/^{39}Ar$ ages have been measured on the same sample there is a significant difference between the ages, which is most likely due to slight sample heterogeneity. In these cases we place more confidence in the $^{40}Ar/^{39}Ar$ total fusion ages since they are measured on a single aliquot of sample.

Table 2. $^{40}Ar/^{39}Ar$ step heating data for samples from the LHC.

A-23 biotite. $^{40}Ar/^{39}Ar$ step heating analyses (ANU no. 93-695)

Temp (°C)	^{36}Ar ($\times10^{-16}$mol)	^{37}Ar ($\times10^{-14}$mol)	^{39}Ar ($\times10^{-13}$mol)	^{40}Ar ($\times10^{-12}$mol)	$^{40}Ar^*$ %	$^{40}Ar^*/^{39}K$	Cumulative ^{39}Ar(%)	Age(Ma) $\pm(1\sigma)$	Ca/K ($\times10^{-3}$)
550	138.40	5.708	1.029	0.5456	25.0	13.25	1.73	240.5±2.5	105.0
625	13.19	11.340	1.014	0.2490	84.3	20.69	3.44	362.9±1.1	212.0
660	17.17	4.174	2.114	0.6078	91.6	26.33	7.01	450.2±1.0	37.5
690	11.49	3.122	3.203	0.8923	96.1	26.77	12.40	456.9±0.3	18.5
720	6.085	3.310	4.423	1.219	98.4	27.14	19.86	462.4±0.3	14.2
740	3.832	3.227	4.767	1.316	99.0	27.34	27.89	465.4±0.3	12.9
760	3.385	2.675	5.049	1.395	99.2	27.41	36.40	466.5±0.4	10.1
790	3.533	3.739	5.771	1.599	99.3	27.50	46.13	467.9±0.3	12.3
830	3.325	3.916	5.120	1.426	99.2	27.63	54.76	469.9±0.3	14.5
880	3.641	0.08656	4.673	1.310	99.1	27.78	62.64	472.0±0.4	0.35
940	5.238	0.08668	6.315	1.806	99.0	28.32	73.28	480.1±0.4	0.26
980	4.127	3.905	5.215	1.478	99.1	28.08	82.07	476.5±0.3	14.2
1050	4.950	4.695	8.436	2.334	99.3	27.47	96.29	467.3±0.6	10.6
1300	1.848	2.735	2.203	0.6082	99.0	27.33	100.00	465.3±0.4	23.6
Total	220.2	52.720	59.330	16.790		27.17		462.9±0.5	

$\lambda = 5.543\times10^{-10}a^{-1}$, $J = 1.0766\times10^{-2}$, Flux Monitor-GA1550 biotite (age=97.9±0.7 Ma)

A-34 hornblende. $^{40}Ar/^{39}Ar$ step heating analyses (ANU no. 93-695)

Temp (°C)	^{36}Ar ($\times10^{-16}$mol)	^{37}Ar ($\times10^{-14}$mol)	^{39}Ar ($\times10^{-13}$mol)	^{40}Ar ($\times10^{-12}$mol)	$^{40}Ar^*$ %	$^{40}Ar^*/^{39}K$	Cumulative ^{39}Ar(%)	Age(Ma) $\pm(1\sigma)$	Ca/K ($\times10^{-3}$)
700	4.273	9.418	0.1062	0.7092	83.5	56.15	0.38	847.1±29.4	17.0
850	1.728	3.808	0.1922	0.7135	93.3	34.70	1.06	568.4± 7.0	3.8
900	0.3402	1.630	0.1034	0.3445	97.5	32.52	1.42	537.5± 7.9	3.0
940	0.9934	7.887	0.3859	1.251	98.2	31.91	2.80	528.7± 3.4	3.9
960	5.262	42.60	1.865	5.554	97.9	29.20	9.42	489.4± 1.4	4.4
970	5.118	49.16	2.135	6.295	98.3	29.04	17.00	487.0± 0.4	4.4
980	3.984	37.90	1.647	4.855	98.3	29.03	22.84	486.9± 0.5	4.4
990	2.945	26.86	1.158	3.412	98.2	28.96	26.96	486.0± 0.6	4.4
1010	9.609	101.20	4.360	12.80	98.5	28.99	42.43	486.3± 0.4	4.4
1020	9.704	106.30	4.577	13.47	98.6	29.07	58.68	487.4± 0.4	4.4
1030	6.909	74.63	3.246	9.595	98.6	29.19	70.21	489.3± 0.5	4.4
1040	5.855	62.16	2.704	8.042	98.6	29.36	79.81	491.8± 0.4	4.4
1050	3.482	39.16	1.694	5.038	98.7	29.40	85.82	492.3± 0.6	4.4
1070	2.534	25.46	1.064	3.178	98.4	29.45	89.59	493.2± 0.6	4.6
1100	3.238	33.46	1.283	3.822	98.3	29.34	94.15	491.5± 0.6	5.0
1400	4.173	48.38	1.649	4.931	98.4	29.50	100.00	493.8± 0.5	5.6
Total	70.15	670.1	28.17	84.01		29.36		491.8± 0.8	

$\lambda = 5.543\times10^{-10}a^{-1}$, $J = 1.0673\times10^{-2}$, Flux Monitor-77-600 hornblende (age=414.1±3.9 Ma)

Austhovde is located on the western side of Lützow-Holm Bay on the Prince Harold Coast, at 69°42′S, 37°47′E. An area ~2 km long and < 500 m wide is exposed at the crest of predominantly ice-covered coastal cliffs. A variety of lithologies make up a well-layered gneiss sequence including biotite gneiss, garnet-biotite gneiss, leucocratic garnet gneiss, gneissic granite, pyroxene gneiss, hornblende gneiss and marble. Narrow (15 cm

Table 2. (Continued).

A-48 biotite. $^{40}Ar/^{39}Ar$ step heating analyses (ANU no. 93-607)

Temp (°C)	^{36}Ar ($\times 10^{-16}$mol)	^{37}Ar ($\times 10^{-14}$mol)	^{39}Ar ($\times 10^{-13}$mol)	^{40}Ar ($\times 10^{-12}$mol)	$^{40}Ar^*$ %	$^{40}Ar^*$ /^{39}K	Cumulative ^{39}Ar(%)	Age(Ma) $\pm(1\sigma)$	Ca/K ($\times 10^{-3}$)
550	135.4	1.896	2.320	0.9675	58.6	24.43	2.78	419.1± 1.1	15.5
650	39.13	4.023	5.782	1.842	93.6	29.84	9.72	500.1± 1.7	13.2
690	19.88	6.547	14.61	4.538	98.6	30.64	27.26	511.8± 0.6	8.52
720	5.941	14.28	16.91	5.231	99.6	30.80	47.56	514.1± 0.6	16.0
750	3.321	9.881	14.51	4.521	99.7	31.07	64.97	518.1± 0.7	12.9
780	2.301	4.886	8.414	2.643	99.7	31.31	75.07	521.5± 0.5	11.0
810	1.362	3.622	3.636	1.148	99.6	31.43	79.43	523.2± 0.4	18.9
840	0.7769	3.267	2.362	0.7431	99.6	31.34	82.27	521.9± 0.4	26.3
890	1.593	2.988	3.260	1.028	99.5	31.35	86.18	522.2± 0.3	17.4
930	2.075	3.889	4.318	1.366	99.5	31.47	91.36	523.9± 0.8	17.1
980	2.713	3.880	3.874	1.239	99.3	31.74	96.01	527.8± 0.4	19.0
1030	1.094	3.588	2.482	0.7899	99.5	31.68	98.99	526.8± 1.2	27.5
1100	0.4023	3.325	0.7483	0.2370	99.4	31.50	99.89	524.2± 0.9	84.4
1300	1.265	1.563	0.09048	0.02851	86.9	27.37	100.00	463.7±20.6	328.0
Total	217.30	67.63	83.31	26.32		30.80		514.11±0.7	

$\lambda = 5.543 \times 10^{-10} a^{-1}$, $J = 1.0706 \times 10^{-2}$, Flux Monitor-GA1550 biotite(age=97.9±0.7 Ma)

R-15 hornblende. $^{40}Ar/^{39}Ar$ step heating analyses (ANU no. 93-574)

Temp (°C)	^{36}Ar ($\times 10^{-16}$mol)	^{37}Ar ($\times 10^{-14}$mol)	^{39}Ar ($\times 10^{-13}$mol)	^{40}Ar ($\times 10^{-12}$mol)	$^{40}Ar^*$ %	$^{40}Ar^*$ /^{39}K	Cumulative ^{39}Ar(%)	Age(Ma) $\pm(1\sigma)$	Ca/K ($\times 10^{-3}$)
700	7.336	0.579	1.126	1.160	81.8	84.6	0.62	1158.0± 7.0	9.8
850	2.607	0.230	0.865	0.742	89.9	77.3	1.10	1082.0± 7.9	5.1
900	0.617	0.142	0.487	0.199	91.5	37.5	1.37	605.9±12.1	5.6
940	1.476	0.690	1.854	0.621	94.0	31.6	2.40	522.7± 4.3	7.1
960	1.393	1.179	2.914	0.908	96.7	30.2	4.02	503.0± 2.6	7.7
980	2.622	2.770	6.757	2.050	97.5	29.7	7.76	495.0± 1.0	7.8
990	1.900	2.110	5.194	1.574	97.7	29.7	10.64	495.5± 1.1	7.7
1000	1.321	1.470	3.831	1.164	97.9	29.8	12.76	496.9± 1.6	7.3
1010	1.591	1.825	4.924	1.486	98.0	29.7	15.49	494.6± 1.5	7.1
1020	2.610	2.762	7.837	2.348	97.8	29.4	19.83	490.7± 0.8	6.7
1030	3.522	4.252	12.450	3.727	98.3	29.5	26.73	492.4± 0.6	6.5
1040	3.050	3.243	9.619	2.881	97.9	29.4	32.07	490.9± 0.9	6.4
1050	2.295	2.744	7.974	2.399	98.3	29.6	36.49	494.4± 0.7	6.6
1060	2.978	3.552	10.700	3.209	98.3	29.6	42.42	493.2± 0.8	6.3
1070	1.772	2.206	6.561	1.958	98.4	29.4	46.05	491.3± 1.4	6.4
1080	1.858	2.156	6.316	1.892	98.2	29.5	49.56	492.0± 0.9	6.5
1100	5.885	7.150	21.180	6.327	98.3	29.5	61.30	491.6± 0.5	6.4
1110	3.400	3.997	11.900	3.548	98.2	29.4	67.89	490.5± 0.6	6.4
1120	3.208	4.006	11.840	3.532	98.4	29.4	74.45	491.3± 1.2	6.4
1130	3.634	4.269	12.560	3.742	98.2	29.4	81.41	490.1± 0.7	6.5
1140	3.422	4.531	13.350	3.984	98.5	29.5	88.81	492.1± 0.5	6.5
1150	2.483	3.245	9.525	2.847	98.5	29.5	94.09	492.6± 0.7	6.5
1170	2.346	3.092	6.861	2.070	98.1	29.7	97.89	495.3± 0.9	8.6
1400	1.471	1.665	3.804	1.152	97.6	29.7	100.00	494.7± 1.6	8.4
Total	64.800	63.860	180.400	55.520		30.1		501.5± 1.0	

$\lambda = 5.543 \times 10^{-10} a^{-1}$, $J = 1.0634 \times 10^{-2}$, Flux Monitor-77-600 hornblende (age=414.1±3.9 Ma)

Table 2. (Continued).

K-12 biotite. $^{40}Ar/^{39}Ar$ step heating analyses (ANU no. 93-515)

Temp (°C)	^{36}Ar ($\times10^{-16}$mol)	^{37}Ar ($\times10^{-14}$mol)	^{39}Ar ($\times10^{-13}$mol)	^{40}Ar ($\times10^{-12}$mol)	$^{40}Ar^*$ %	$^{40}Ar^*/^{39}K$	Cumulative ^{39}Ar(%)	Age(Ma) $\pm(1\sigma)$	Ca/K ($\times10^{-3}$)
500	273.6	0.007683	0.5691	0.9479	14.7	24.49	1.16	415.9±6.6	2.6
550	42.16	0.2171	0.3320	0.1894	34.2	19.50	1.84	338.6±4.8	124.0
600	50.06	0.3315	0.5959	0.2778	46.7	21.77	3.06	374.3±2.5	106.0
650	103.0	0.09689	2.734	1.082	71.8	28.41	8.64	474.4±0.8	6.7
700	46.30	0.007670	7.041	2.156	93.6	28.65	23.02	478.0±0.5	0.2
740	8.228	0.007670	7.816	2.268	98.8	28.68	38.98	478.4±0.3	0.19
755	3.585	0.07903	5.142	1.488	99.2	28.71	49.48	478.9±0.4	2.9
770	2.155	0.3009	3.855	1.119	99.3	28.85	57.36	480.9±0.5	14.8
790	3.415	0.2951	3.173	0.9272	98.8	28.88	63.84	481.3±0.5	17.7
810	0.8787	0.1387	2.195	0.6437	99.5	29.18	68.32	485.8±0.4	12.0
850	2.895	0.3652	2.462	0.7297	98.7	29.26	73.35	486.9±0.6	28.2
890	3.889	0.3700	3.943	1.173	89.9	29.43	81.40	489.3±1.9	17.8
920	2.930	0.3738	3.268	0.9677	99.0	29.33	88.07	487.9±0.6	21.7
950	1.954	0.7865	2.385	0.7066	99.1	29.36	92.94	488.3±0.4	62.6
1050	3.633	7.3190	3.362	0.9905	98.9	29.14	99.81	485.2±0.4	414.0
1300	0.5803	0.8023	0.09342	0.02994	94.5	30.30	100.00	502.0±9.8	1630.0
Total	549.3	11.50	48.97	15.70		28.72		479.0±0.7	

$\lambda = 5.543\times10^{-10}a^{-1}$, $J = 1.0588\times10^{-2}$, Flux Monitor-GA1550 biotite(age=97.9±0.7 Ma)

K-12 hornblende. $^{40}Ar/^{39}Ar$ step heating analyses (ANU no. 93-515)

Temp (°C)	^{36}Ar ($\times10^{-16}$mol)	^{37}Ar ($\times10^{-14}$mol)	^{39}Ar ($\times10^{-13}$mol)	^{40}Ar ($\times10^{-12}$mol)	$^{40}Ar^*$ %	$^{40}Ar^*/^{39}K$	Cumulative ^{39}Ar(%)	Age(Ma) $\pm(1\sigma)$	Ca/K ($\times10^{-3}$)
700	29.38	31.96	0.3556	7.525	88.9	189.4	0.80	1987±2.2	17.2
800	4.202	3.665	0.1866	3.098	96.1	159.8	1.22	1788±4.3	3.7
850	2.231	2.898	0.1183	1.115	94.3	89.13	1.48	1200±5.0	4.7
880	1.924	3.015	0.1059	1.181	95.4	106.6	1.72	1346±5.6	5.4
910	4.181	15.95	0.3734	3.479	96.9	90.58	2.56	1214±2.6	8.1
940	5.547	70.75	1.420	7.330	98.7	51.15	5.75	781.6±0.6	9.5
960	8.424	147.0	2.968	11.49	99.1	38.52	12.42	617.7±0.4	9.5
980	17.30	333.2	6.840	23.69	99.2	34.50	27.79	562.3±0.4	9.3
990	9.474	190.0	3.909	12.66	99.3	32.27	36.57	530.8±0.4	9.3
1000	8.32	178.4	3.688	11.61	99.4	31.40	44.86	518.4±0.4	9.2
1010	8.342	180.6	3.775	11.77	99.4	31.11	53.34	514.2±1.3	9.1
1020	7.724	175.8	3.735	11.53	99.5	30.84	61.73	510.3±0.3	9.0
1030	5.863	134.6	2.911	8.996	99.5	30.87	68.28	510.8±0.3	8.8
1050	8.897	176.5	3.878	12.19	99.3	31.32	76.99	517.2±0.4	8.7
1080	15.50	310.0	6.716	22.75	99.3	33.76	92.08	552.0±0.4	8.8
1100	5.62	123.1	2.655	9.339	99.5	35.13	98.05	571.1±0.6	8.8
1150	1.602	30.68	0.6623	2.368	99.3	35.62	99.54	577.9±1.0	8.8
1400	0.4518	9.402	0.2053	0.7327	99.4	35.62	100.00	577.9±3.6	8.7
Total	145.0	2118.0	44.5	162.9		36.233		586.4±0.6	

$\lambda = 5.543\times10^{-10}a^{-1}$, $J = 1.0601\times10^{-2}$, Flux Monitor-77-600 hornblende (age=414.1±3.9 Ma)

Table 2. (Continued).

CH-15 biotite. $^{40}Ar/^{39}Ar$ step heating analyses (ANU no. 93-551)

Temp (°C)	^{36}Ar ($\times 10^{-16}$mol)	^{37}Ar ($\times 10^{-14}$mol)	^{39}Ar ($\times 10^{-13}$mol)	^{40}Ar ($\times 10^{-12}$mol)	$^{40}Ar^*$ %	$^{40}Ar^*/^{39}K$	Cumulative ^{39}Ar(%)	Age(Ma) $\pm(1\sigma)$	Ca/K ($\times 10^{-3}$)
550	33.21	0.6618	1.184	0.3903	74.8	24.64	2.39	425.3±1.1	10.6
630	27.35	3.093	4.959	1.447	94.3	27.52	12.39	469.0±0.4	11.9
670	6.974	0.09144	7.944	2.252	99.0	28.07	28.41	477.2±0.4	0.219
690	2.758	4.799	8.747	2.480	99.6	28.24	46.05	479.8±0.3	10.4
710	2.168	0.1049	9.666	2.746	99.7	28.31	65.55	480.9±0.7	0.206
725	1.345	4.533	6.748	1.916	99.7	28.31	79.16	480.8±0.3	12.8
740	0.7769	2.243	4.080	1.162	99.7	28.40	87.39	482.1±0.4	10.4
770	0.5989	1.430	1.884	0.5376	99.6	28.41	91.19	482.3±0.4	14.4
830	0.7474	1.144	1.341	0.3818	99.3	28.28	93.90	480.4±0.6	16.2
900	0.8203	0.8407	1.663	0.4717	99.4	28.19	97.25	479.1±0.6	9.6
950	0.6575	0.9241	1.260	0.3581	99.4	28.23	99.79	479.7±0.5	13.9
1100	0.5923	0.09551	0.1028	0.03149	99.4	28.92	100.00	489.8±6.2	17.7
Total	78.01	19.96	49.58	14.17		28.10		477.7±0.5	

$\lambda = 5.543 \times 10^{-10} a^{-1}$, $J = 1.0788 \times 10^{-2}$, Flux Monitor-GA1550 biotite(age=97.9±0.7 Ma)

BT-1 biotite. $^{40}Ar/^{39}Ar$ step heating analyses (ANU no. 93-1260)

Temp (°C)	^{36}Ar ($\times 10^{-16}$mol)	^{37}Ar ($\times 10^{-14}$mol)	^{39}Ar ($\times 10^{-13}$mol)	^{40}Ar ($\times 10^{-12}$mol)	$^{40}Ar^*$ %	$^{40}Ar^*/^{39}K$	Cumulative ^{39}Ar(%)	Age(Ma) $\pm(1\sigma)$	Ca/K ($\times 10^{-3}$)
500	6.747	0.3796	0.07507	0.3141	36.6	15.32	0.25	279.18±8.7	961.0
600	8.285	0.1015	0.3217	0.5439	54.8	9.27	1.30	174.12±6.0	60.0
690	11.20	0.08096	1.253	3.679	90.9	26.69	5.40	461.73±0.6	12.3
720	5.876	0.3722	2.407	6.727	97.3	27.20	13.28	469.47±0.5	29.4
740	3.990	0.3982	3.184	8.777	98.6	27.17	23.71	468.94±0.3	23.8
760	2.440	0.8775	3.473	9.527	99.2	27.20	35.08	469.47±0.3	48.0
780	1.536	0.1906	2.912	7.987	99.3	27.24	44.61	470.07±0.4	12.4
810	0.6354	0.06348	2.318	6.383	99.6	27.43	52.20	472.92±0.6	5.20
850	0.7654	0.07351	2.014	5.556	99.5	27.45	58.80	473.20±0.4	6.93
890	1.485	0.1409	1.868	5.160	99.1	27.36	64.91	471.84±0.4	14.3
940	1.765	0.2820	1.971	5.489	99.0	27.56	71.36	474.96±0.6	27.2
1000	2.553	0.02125	3.942	10.97	99.2	27.61	84.27	475.61±0.6	1.02
1150	2.998	0.4471	4.538	12.49	99.2	27.30	99.13	470.89±0.4	18.7
1300	2.216	0.06486	0.2665	0.8186	91.9	28.24	100.00	485.18±5.8	46.2
Total	52.50	3.4940	30.54	84.42		27.105		468.0 ±0.6	

$\lambda = 5.543 \times 10^{-10} a^{-1}$, $J = 1.0926 \times 10^{-2}$, Flux Monitor-GA1550 biotite (age=97.9 ±0.7 Ma)

wide) amphibolite dykes cross-cut the gneissic layering and are in turn cross-cut by coarse pegmatite.

3.1.1. Structure

Most rocks show a strong gneissic fabric trending north-south and dipping east. The internal parts of boudins of mafic pyroxene gneiss sitting within biotite and garnet-biotite gneiss often show a pre-existing fabric which is not parallel to the dominant gneissic layering. Open folding of the gneissic layering generates a gently northwest plunging mineral lineation defined by biotite and hornblende. Gneissic granite in the southwest of Austhovde shows contacts with surrounding hornblende gneiss which are generally

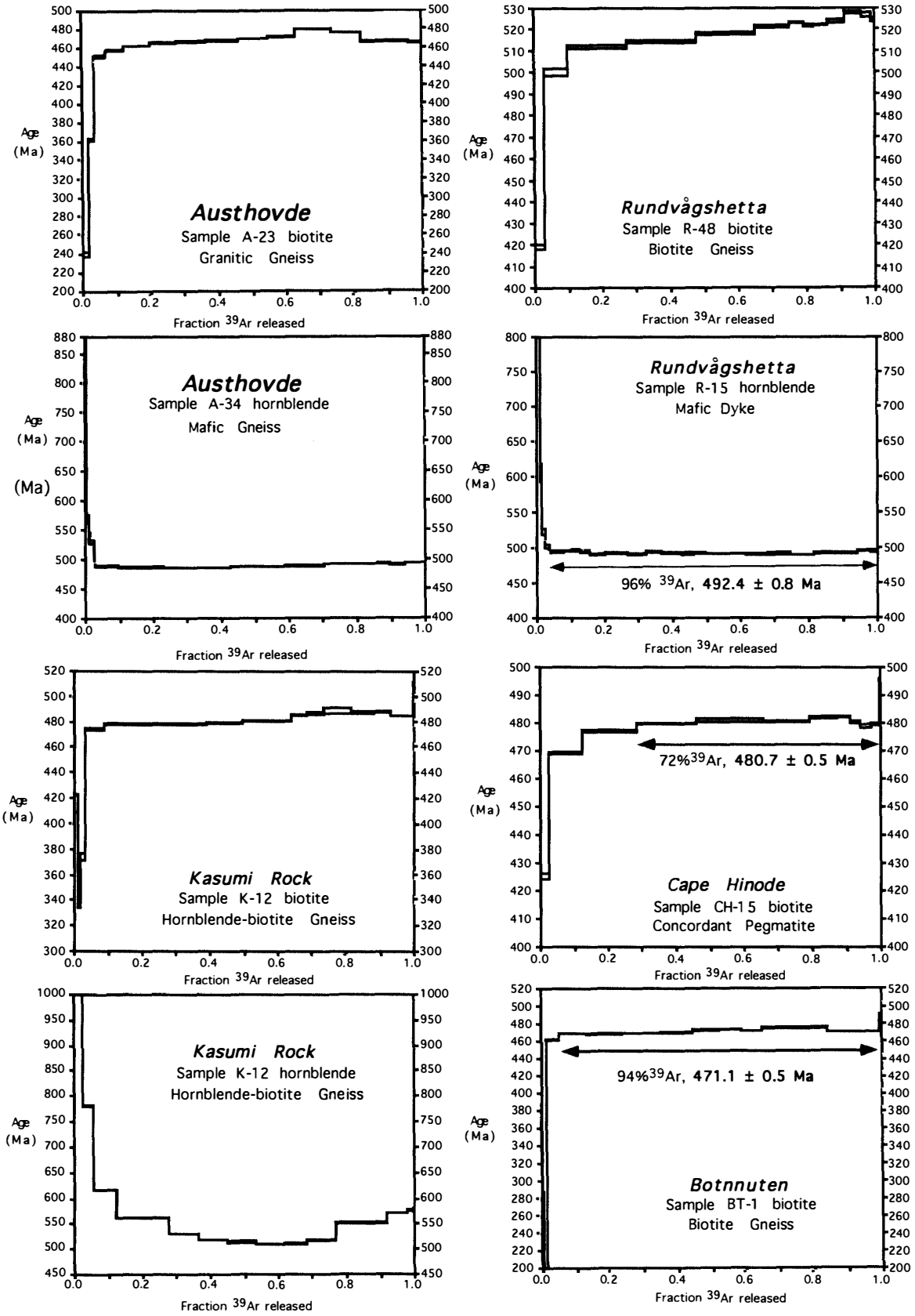

Fig. 2. $^{40}Ar/^{39}Ar$ *age spectra as discussed in text.*

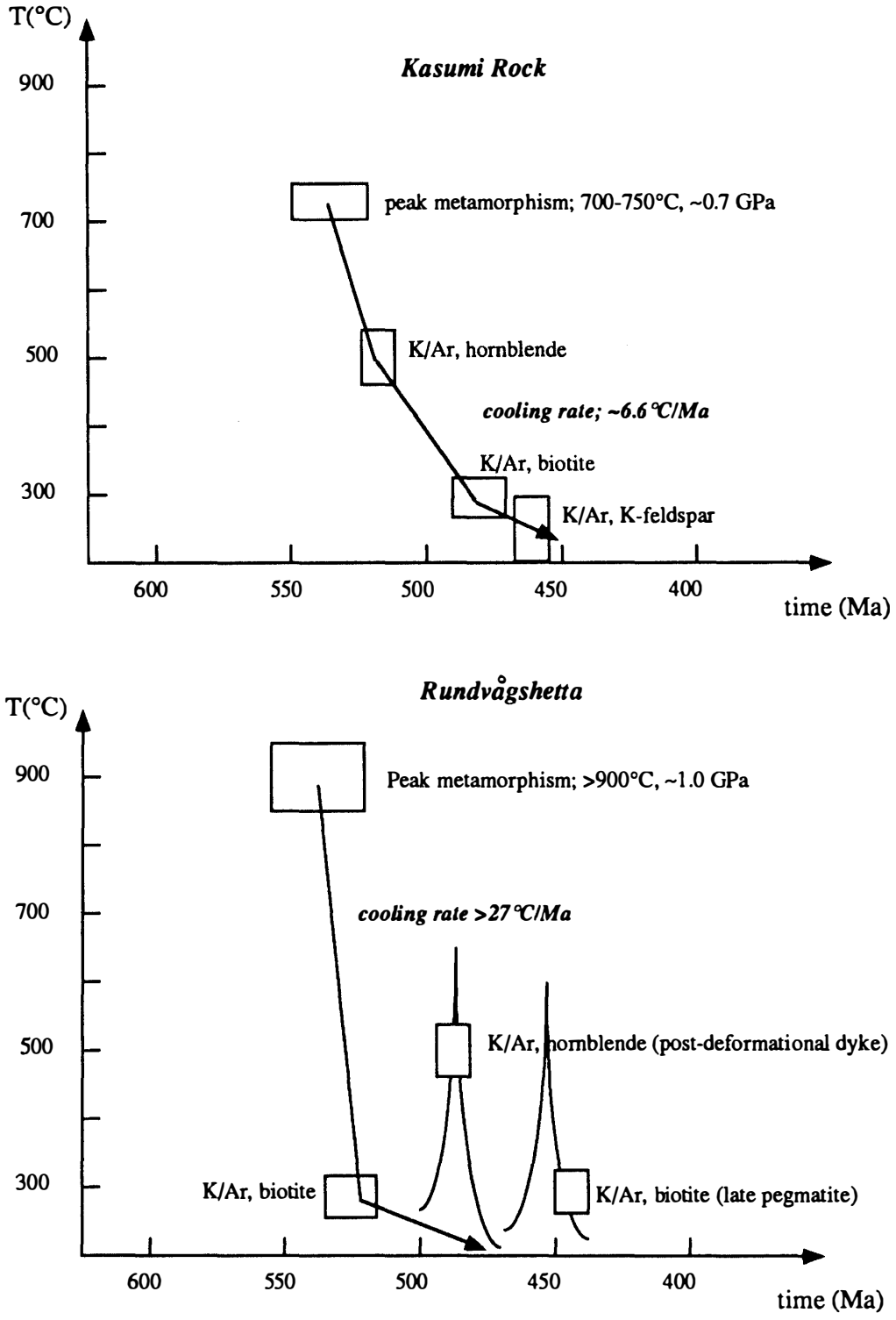

Fig. 3. Temperature versus time cooling curves for four localities in the LHC. Peak metamorphic conditions come from the estimates of MOTOYOSHI *(1993), timing of peak metamorphism is assumed to be given by the timing of final zircon growth ages after* SHIRAISHI *et al. (1994), and work in progress, and cooling ages come from the K/Ar and $^{40}Ar/^{39}Ar$ results of this study. Closure temperatures for the respective minerals in the K/Ar system are taken to be; hornblende ~500 ±*

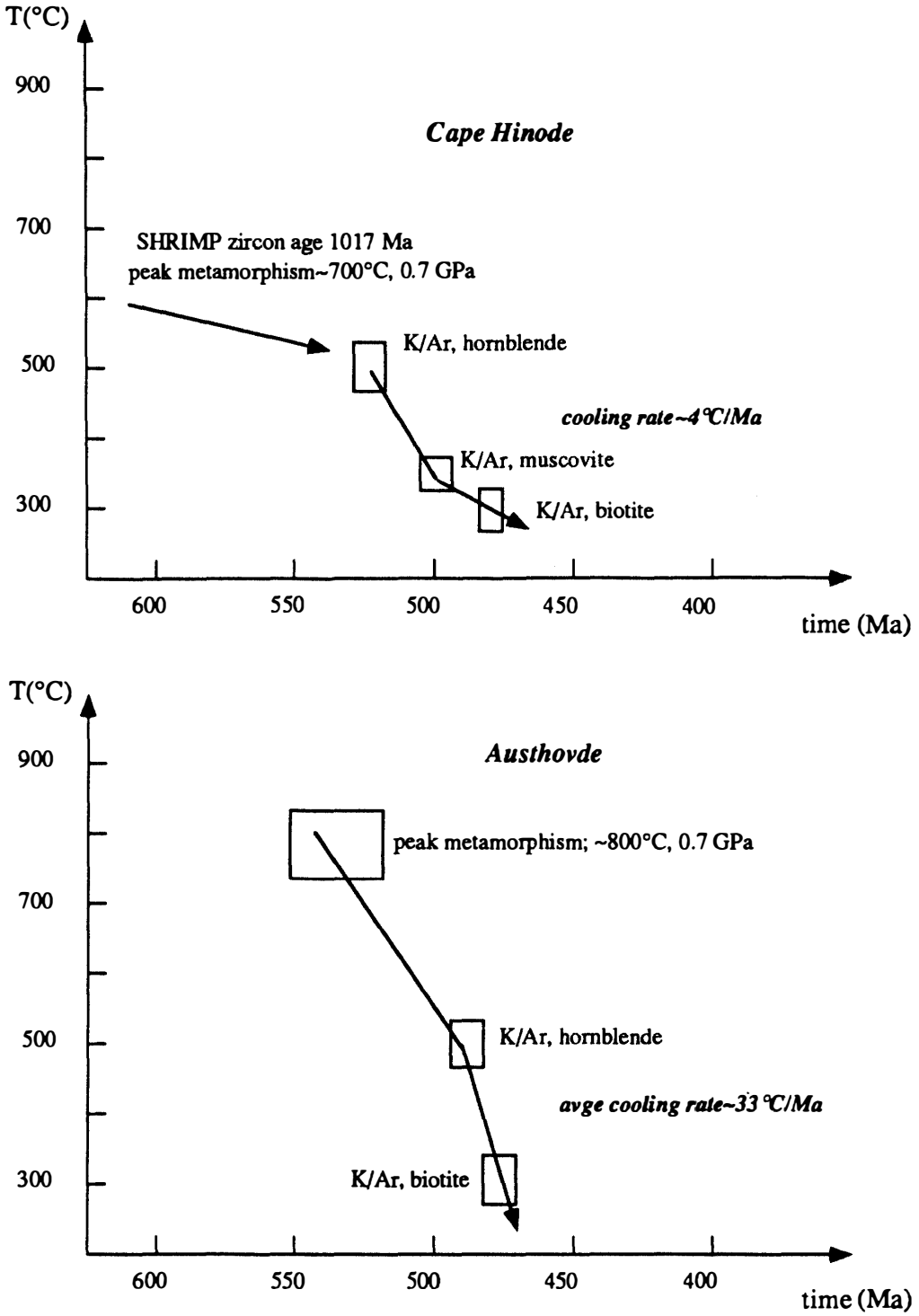

30°C, muscovite ~350±30°C, biotite ~300±30°C, K-feldspar ~225±75°C. Note that the cooling rates given in this figure for Kasumi Rock, Cape Hinode and Austhovde are average values for the period between hornblende closure and biotite closure. For Kasumi Rock this rate is slightly lower than average cooling rate from peak metamorphism to the time of biotite closure as calculated in Table 3.

concordant, but in some places cross-cut the gneissic fabric. The gneissosity itself is well developed in the gneissic granite and is continuous across the contacts. The intrusion of the gneissic granite therefore predates the generation of the gneissic fabric at Austhovde. Late stage discordant pegmatites post-date all other structure at Austhovde.

3.1.2. Samples from Austhovde

A-23 (ANU no. 93-675) This is the gneissic granite referred to above. It is an orange rock, composed of quartz-plagioclase-K-feldspar-biotite and exhibits a strong gneissic layering defined by thin (<1 cm) layers and streaks of biotite±hornblende through the otherwise dominantly felsic matrix. Within the mafic layers, the minerals are fairly randomly oriented. This rock sits within dark grey hornblende gneiss. Biotite from the gneissic granite gives a K/Ar age of 449±5 Ma. $^{40}Ar/^{39}Ar$ step heating on the same biotite produces an age spectrum which rises monotonically to a maximum apparent age of 480.1±0.4; the integrated total fusion age is 463±1 Ma.

A-34 (ANU no. 93-695) This sample is a pyroxene-garnet gneiss which forms boudinaged layers in the gneiss sequence at Austhovde. Hornblende from this rock yields a K/Ar age of 502±5 Ma; step heating reveals very minor excess argon in the hornblende but with an overall flat age spectrum. The minimum apparent age of 486.0±0.6 Ma is therefore regarded as a good approximation of the time of closure of hornblende.

3.1.3. Discussion of ages from Austhovde

The hornblende and biotite samples from Austhovde are both derived from gneissic rocks, and the ages are therefore interpreted simply as cooling ages for the gneissic sequence. Taking the maximum apparent biotite age of 480 Ma, and the minimum apparent hornblende age of 486 Ma, as best estimates for closure of these minerals gives an average cooling rate between ~500 and 300°C of about ~33°C/Ma.

3.2. Botnnuten

Botnnuten is a spectacular nunatak which rises 500 m vertically above the continental ice-sheet at an elevation of 1000 m, approximately 70 km southwest of Lützow-Holm Bay, lat. 70°24′S, long. 38°01′E. This is the only inland exposure of basement rock in this region of Antarctica other than the Yamato-Belgica complex which lies more than 200 km further to the southwest. Lithologically and petrographically Botnnuten appears to belong to the LHC (MOTOYOSHI and SHIRAISHI, 1985) being composed of flat lying, interlayered biotite gneiss, biotite-garnet gneiss, garnet-sillimanite gneiss, garnet-pyroxene gneiss, impure marble and calcsilicate. A sample of the typical felsic biotite-garnet-gneiss from Botnnuten (BT-1, ANU no. 93-1260) yields a K/Ar age on biotite of 474±5 Ma. $^{40}Ar/^{39}Ar$ step heating is consistent with this K/Ar age, with 94% of the ^{39}Ar released in 10 consecutive steps in the temperature interval 720 to 1150°C, with a combined age of 471.1±0.5 Ma (Fig. 2).

3.3. Rundvågshetta

Rundvågshetta forms an ice-free headland ~6 km² in area, located at 69°54′S and 39°01′E, in the southern part of Lützow-Holm Bay. Rocks from this locality define the metamorphic thermal maximum of HIROI *et al.* (1991), and MOTOYOSHI *et al.* (1993) have estimated that peak metamorphic conditions exceeded 900°C at ~1.0 GPa. For a detailed description of the structure at Rundvågshetta see ISHIKAWA *et al.* (1994). The rocks

consist of interlayered gneisses ranging in composition from a relatively felsic garnet-gneiss, through garnet-biotite and biotite-hornblende gneisses to mafic pyroxene gneiss. Pelitic, sillimanite-bearing gneiss is common, particularly on the northern shore platform. Within the concordant layered gneisses sit blocks and lenses of boudinaged mafic and ultramafic rock, usually 1-3 m wide and up to 10 m in strike length. In the southern part of Rundvågshetta two sets of narrow (< 1 m wide) mafic dykes cross-cut the gneiss sequence. Two pegmatite phases are recognised, one broadly concordant to gneissic layering and the other sharply cross-cutting.

3.3.1. Structure

The gneiss sequence at Rundvågshetta trends WNW with variable dip. Variation in dip is due to broad, upright, open to tight folds which form a large antiform in the northern part of the area. An upright axial planar, biotite fabric has developed in association with these folds, and can be found pervasively across the area. Fold axes trend WNW and are subhorizontal, but minor variations in plunge, in combination with topography result in some complex surface outcrop patterns. At least two phases of intense ductile deformation, producing isoclinal folds and a strong gneissic fabric, predate these open-tight folds.

Coarse-grained leucocratic patches and veins of melt occur within biotite gneisses parallel to the gneissic layering on scales ranging from millimetres to several centimetres in width. Sheet-like pegmatites of coarse-grained plagioclase-quartz-K-feldspar-biotite, up to 2 m wide, lie concordant to the gneissic layering. Contacts between the pegmatite and the gneiss are irregular and gradational, and often show a selvage enriched in coarse biotite. These pegmatites follow the layering concordantly around upright folds, but do not contain the axial planar biotite fabric which is seen in the surrounding gneisses. The concordant pegmatite phase is interpreted to be the result of segregation of local partial melts of the surrounding gneisses, and is therefore regarded as coeval with pervasive heating of the terrain. It post-dates the early, intense, isoclinal deformation, but predates upright folding. The concordant pegmatite phase at Rundvågshetta morphologically resembles the "migmatitic" pegmatite described from Kasumi Rock, and shows very similar relative timing relations with deformational and intrusive events in the surrounding rocks.

In the southern part of Rundvågshetta two sets of narrow, steeply dipping mafic dykes cross-cut the gneissic layering. The first phase is composed of clinopyroxene-hornblende-plagioclase and variable amounts of biotite. It is generally dark green in the core with a black, hornblende rich rim, and forms parallel sets trending N-S. This phase is cross-cut by light grey dykes composed of hornblende-biotite and minor plagioclase. These trend NE-SW. Both sets of dykes are relatively undeformed and can be traced for tens to hundreds of metres across strike.

The last event at Rundvågshetta was the intrusion of vertical dykes of pegmatite. These dykes are most common in the northern part of Rundvågshetta. They are steeply dipping to vertical, occur in parallel sets trending roughly north-south and can be traced across strike for over 100 m maintaining a constant width of 1-3 m. They cross-cut the gneissic layering with sharp, linear margins. Volumetrically the late pegmatites are much less significant than the concordant, pegmatitic melts.

3.3.2. Samples from Rundvågshetta

R-47 (ANU no. 93-606) This sample is from a coarse, grained, concordant pegmatite, consisting of plagioclase, quartz, K-feldspar and biotite. The rock is internally unstructur-

ed, and has a patchy pink and white appearance due to the distribution of K-feldspar. This pegmatite forms a sheet-like body, 1–2 m thick, broadly concordant with the surrounding biotite gneiss. Biotite from this rock gives an age of 500±5 Ma.

R-48 (ANU no. 93–607) This is a felsic biotite gneiss dominantly composed of quartz and plagioclase, with minor K-feldspar. Biotite occurs throughout this rock but is concentrated in thin (<0.5 cm wide) bands which often also contain minor garnet, and which define the gneissic layering. This is the dominant rock type at Rundvågshetta, and is interlayed with metaquartzites, metapelites and metabasites. R-48 was collected approximately 1 m from sample R-47. Biotite from this rock gives a K/Ar age of 516± 5 Ma and a $^{40}Ar/^{39}Ar$ integrated total fusion age of 514±1 Ma. The $^{40}Ar/^{39}Ar$ age spectrum on biotite (Fig. 2) from this rock rises monotonically to a maximum apparent age of 527.8±0.4 Ma, which represents a minimum estimate for the time of initial closure to argon loss.

R-60 (ANU no. 93–617) This sample comes from the latest phase of linear, cross cutting pegmatites and exhibits an igneous texture consisting of coarse grained plagioclase, quartz, K-feldspar and biotite, plus large magnetite crystals. Biotite from R-60 gives a K/Ar age of 445±5 Ma.

R-15 (ANU no. 93–574) This mafic dyke from Rundvågshetta comes from the earlier of two sets of cross cutting mafic dykes. The mineralogy is clinopyroxene, hornblende and plagioclase showing an unstrained igneous texture. The margins of these dykes are often very rich in biotite. The dykes are locally slightly kinked but maintain a consistent orientation for tens to hundreds of metres across strike. They are therefore regarded as post-dating the regional ductile deformation. Hornblende from R-15 gives a K/Ar age of 512±6 Ma. Step heating reveals minor excess argon and produces a very flat age spectrum (Fig. 2) with 96% of the ^{39}Ar released in 19 consecutive steps in the temperature interval 980 to 1400°C, with a combined age of 492.4±0.8 Ma.

3.3.3. Discussion of ages from Rundvågshetta

The $^{40}Ar/^{39}Ar$ results from sample R-48 suggest that biotite closed to argon loss as early as 528 Ma. Note that this biotite age from the gneiss sequence at Rundvågshetta is significantly older than those from Kasumi Rock, where biotite ages from gneisses range between 492 and 472 Ma. The plateau in the hornblende spectrum from R-15, with an age of ~494 Ma, suggests that this dyke was intruded after regional cooling had taken the terrain below 300°C. This is consistent with the field relations which show the dyke post-dating regional ductile deformation. The late stage, discordant pegmatite (R-60), gives a biotite age of 445 Ma. Since the terrain cooled below 300°C more than 80 Ma prior to this, the pegmatite is likely to have cooled and crystallised rapidly following emplacement. The K/Ar biotite age is therefore regarded as a good estimate of the emplacement age of the pegmatite.

3.4. Berrodden

Berrodden forms another small ice-free headland, located at 69°47′S and 39°07′E, approximately 15 km north of Rundvågshetta in Lützow-Holm Bay. About 2 km² of rock is exposed. Lithology at Berrodden is dominated by leucocratic, garnet-bearing gneiss composed of quartz-plagioclase-K-feldspar-biotite-garnet with thin discontinuous biotite-garnet rich layers and some almost pure quartzite layers. Biotite gneiss, pyroxene

gneiss and marble are interlayered with the leucocratic garnet-gneiss. The southern part of Berrodden consists of dark, red-brown pyroxene gneiss containing small garnets.

3.4.1. Structure

Gneissic layering is relatively flat lying over most of the area, but gently undulates about E-W trending open folds which produce a weak axial planar biotite fabric. The dominant fabric now preserved in the dominantly quartzofeldspathic gneisses is defined by biotite rich trails, often also containing fine grained garnet and parallels larger scale lithological layering. Running along strike in the gneiss sequence are zones of coarse-grained, pegmatitic material regarded as felsic melts. Three of these zones, each between 10 and 20 m wide, can be found at Berrodden within an across-strike distance of ~500 m. Within these zones the dominant rock type is composed of coarse grained plagioclase-quartz-K-feldspar with clots of very coarse biotite distributed throughout. These pegmatites form sheet-like bodies which are concordant with gneissic layering on the map scale but in outcrop the margins of the pegmatites show extensive networks of pegmatitic veins invading the surrounding gneiss. These pegmatites contain no internal fabric and include rafts of the surrounding gneisses. They therefore must post-date the deformation responsible for the dominant, metamorphic fabric. By analogy with the concordant pegmatites from Rundvågshetta (just 15 km along the coast) they are regarded as pre- or syn-upright, gentle folding. Narrow (~1 m wide), linear pegmatites, composed of plagioclase-quartz-K-feldspar-biotite, and with sharp, intrusive contacts, cross-cut the gneissic layering and are regarded as the final structural event in the Berrodden area. Only one sample has been dated from Berrodden. Sample BE-24 (ANU no. 93-644) is from a sheet of semiconcordant, coarse grained pegmatite with biotite giving a K/Ar age of 476±5 Ma.

3.5. Kasumi Rock

Kasumi Rock is located at lat. 68°21.5′S and long. 42°13.3′E on the Prince Olav Coast, approximately 150 km northeast of Syowa Station. An area of approximately 2 km^2 is ice-free, exposing the metamorphic basement rocks on relatively flat, ice-scoured pavements which present 100% exposure. These rocks lie upgrade of the staurolite-out and epidote-quartz out isograds of Hiroi *et al.* (1991), but downgrade of the orthopyroxene-in isograd.

3.5.1. Lithologies

Kasumi Rock is dominantly composed of biotite gneiss, layered on all scales, and grading into more mafic biotite-hornblende gneiss and leucocratic garnet-bearing granitic gneiss. The typical biotite-gneiss is light gray with a plagioclase dominated matrix, plus quartz and minor K-feldspar. Biotite grains are commonly concentrated in thin trails, 1-2 mm wide, defining a gneissic layering, and are generally oriented parallel to these trails. Individual biotite grains are sparsely distributed through the felsic matrix, and are oriented parallel to the gneissosity. Biotite-hornblende gneiss is dark grey and contains a larger percentage of biotite, together with hornblende. In the biotite-hornblende gneiss biotite generally is coarser and is concentrated in broader gneissic layers, up to 2-3 cm wide, and once again is aligned with the layering. In the northern part of the Kasumi Rock outcrop, a highly deformed marble layer forms a structural marker unit varying between 1 and 10 m in thickness. Linear pegmatite dykes of coarse grained plagioclase-quartz-K-feldspar-biotite+large magnetite crystals cross cut the gneissic layering on the northern shore platform at Kasumi Rock. These are approximately 1 m wide, undeformed, vertical dykes

with sharp intrusive contacts, and can be followed across strike for tens to hundreds of metres.

3.5.2. Structure

A strong gneissic fabric is present throughout the region and parallels the large scale lithological variation. Amphibolite lenses can be seen isoclinally folded into parallelism with the gneissic fabric, which is in turn folded about upright, gentle to tight folds. A weak axial planar biotite fabric develops in the nose of these upright folds in biotite rich layers. This fabric is not uniformly developed in layers of different composition-hornblende-biotite gneiss layers do not show this axial planar fabric. The gneissic sequence at Kasumi is extensively migmatised, with leucosome material making up 20–30% of the total rock volume in places. Leucosomes of plagioclase, quartz, and K-feldspar, 1–2 cm wide, are common, and generally parallel the gneissic layering. The leucosomes are commonly rimmed by biotite-rich selvages, and are interpreted as partial melt segregations. In the cores of upright, tight folds, these leucosomes are sometimes aligned along the axial plane of the folds suggesting that partial melting occurred synchronously with upright folding. Elsewhere, layer parallel leucosomes often grade into larger bodies of coarse plagioclase, quartz and K-feldspar, which lie concordant to the gneissic layering but show no internal fabric, and contain coarse clots of biotite randomly oriented throughout. These bodies, described here as migmatitic pegmatite, are generally 1–3 m wide and several tens of metres in strike length and are interpreted to result from larger scale segregation of partial melt from the migmatitic gneisses. Contacts between the migmatitic pegmatite and surrounding gneisses are diffuse rather than sharp. The last structural event at Kasumi Rock was the intrusion of steeply dipping linear pegmatites, with sharp intrusive contacts, cross-cutting the layered gneiss sequence.

3.5.3. Samples from Kasumi Rock

K-12 (ANU no. 93–515) This sample is a hornblende-biotite gneiss interlayed with biotite gneiss. Variation in composition, ranging from dark hornblende-rich/plagioclase-poor layers, through lighter grey hornblende-biotite-plagioclase layers to more felsic biotite-plagioclase layers, defines the gneissic layering. The gneissic layering has experienced early isoclinal folding, and has then been refolded about upright folds which show a weak, axial planar biotite fabric. The development of this axial planar fabric is variable across different compositional layers. In hornblende-rich layers, hornblende shows no reorientation into the axial plane of the upright folds, but is oriented parallel to the gneissic layering and wraps around upright fold hinges. Some layers preserve a preexisting biotite fabric which wraps around the upright folds and show no axial planar fabric, whereas other layers develop a strong axial fabric to these same folds.

Biotite from this rock gives a K/Ar age of 492 ± 5 Ma. Hornblende from the same rock gives a K/Ar age of 599 ± 6 Ma. $^{40}Ar/^{39}Ar$ age spectra from both biotite and hornblende from this rock are shown in Fig. 2. Biotite yields a relatively flat age spectrum which rises monotonically from 474 to 489 Ma while releasing $\sim$78% of the ^{39}Ar. The hornblende age spectrum is distinctly saddle shaped, interpreted as indicating the presence of excess radiogenic argon. Consequently the youngest apparent age of 510.3 ± 0.3 Ma, in the spectrum in the middle of the argon release pattern is regarded as maximum for the closure age of this hornblende.

K-18 (ANU no. 93–521) This sample is a coarse migmatitic segregation in biotite

gneiss. Such segregations typically collect in the necks of metre-scale pinch and swell structures in the gneiss and are interpreted as the same melt phase as larger segregations which make up semi-concordant sheets of migmatitic pegmatite. K-18 was taken from one of these segregations within 2 m of one of the migmatitic pegmatites. The migmatitic segregations consist of a coarse plagioclase-quartz matrix with books of biotite up to 2 cm across randomly oriented throughout. Biotite concentration tends to be highest nearest the margins. This coarse biotite gives a K/Ar age of 481 ± 5 Ma whereas K-feldspar from this rock gives an age of 463 ± 4 Ma.

K-30 (ANU no. 93-533) This sample is from the migmatitic pegmatite phase, which forms large, patchy pink and white bodies and sheets, consisting of coarse plagioclase-quartz-K-feldspar with relatively minor biotite. Biotite separated from this rock gives a K/Ar age of 472 ± 5 Ma.

K-34 (ANU no. 93-536) This sample comes from a coarse grained leucocratic layer in the gneiss sequence. Biotite is sparsely but evenly distributed throughout and forms an axial fabric to upright folds which cross-cuts compositional layering. Biotite gives a K/Ar age of 477 ± 5 Ma.

3.5.4. Discussion of ages from Kasumi Rock

Four K/Ar biotite ages have been obtained from Kasumi Rock, two of which (K-12, K-34) are from layered gneisses and two from partial melts. All four ages lie between 492 ± 5 Ma (K-12) and 472 ± 5 Ma (K-30). Pervasive partial melting implies that temperature in the gneiss sequence must have been >600°C-well above the closure temperature for biotite in the K/Ar system of $\sim$300°C. It could therefore be expected that all four biotite samples should have closed to argon diffusion at the same time during the cooling history. However there is a significant spread in the biotite K/Ar ages over $\sim$20 Ma which is somewhat problematic. HARRISON *et al.* (1985) have shown that the closure temperature of biotite is dependant on the mineral composition, but this effect is unlikely to account for the spread in ages seen here where there is no systematic age variation between biotites from gneisses versus biotites from melts. Biotite is known to undergo structural changes upon heating under vacuum, and it is not clear to what extent the resultant $^{40}Ar/^{39}Ar$ age spectra reflect geologically meaningful age gradients. The detailed interpretation of biotite age spectra is therefore problematic (MCDOUGALL and HARRISON, 1988). In the case of K-12, the best estimate for the time of closure to argon loss could either be regarded as $\sim$479 Ma (the flattest part of the age spectrum, and the total fusion age), or the maximum apparent age of 489 Ma could be taken as the time of initial closure with some subsequent minor argon loss, possibly as a result of relatively slow cooling through the closure temperature interval. For consistency with our interpretation of biotite age spectra from Austhovde and Rundvågshetta, we once again take the maximum apparent age (489 Ma) as an estimate for time of closure when calculating cooling rate in Table 3. The closure temperature of K-feldspar is not well constrained. Indeed K-feldspar may well exhibit a range of closure temperatures between $\sim$150-300°C, corresponding to different diffusion domains (LOVERA *et al.*, 1989). The K-feldspar age of 463 ± 4 Ma is slightly younger than the youngest of the biotite ages, consistent with K-feldspar not finally closing to argon diffusion until a somewhat lower temperature than biotite. The hornblende $^{40}Ar/^{39}Ar$ age spectrum suggests a maximum age for isotopic closure of hornblende of $\sim$510 Ma.

Based on commonly accepted values for closure temperature to argon loss of $\sim$500°C

Table 3. Calculation of average cooling and exhumation rates for three localities in the LHC, based on assumptions discussed in the text.

Locality	t_{peak} (Ma)	T_{peak} (°C)	P_{peak} (GPa(km))	t_{bio} (Ma)	T_{bio} (°C)	P_{bio} (GPa(km))	cooling rate (°C/Ma)	exhumation rate (mm/yr)
Austhovde	550-520	~800	~0.7(24)	480	300	0.4(13)	7.1-12.5	0.16-0.28
Botnnuten	550-520	750	~0.55(18)	473	300	0.4(13)	5.8-9.6	0.06-0.11
Rundvågshetta	550-520	>900	~1.0(35)	528	300	0.4(13)	>27	>1.0
Kasumi Rock	550-520	~700	~0.7(24)	480	300	0.4(13)	5.7-10	0.16-0.28

t_{peak} is the time of peak metamorphism, T_{peak} and P_{peak} are the temperature and pressure at peak metamorphism respectveely, t_{bio} is the time of biotite closure to argon loss (as measured by K/Ar or $^{40}Ar/^{39}Ar$ ages), T_{bio} is the closure temperature of biotite, and P_{bio} is the closure pressure of biotite assuming a standard geotherm (see text). Cooling rates are calculated simply as $(T_{peak}/T_{bio})/(t_{peak}/t_{bio})$, and exhumation rates as $(P_{peak}-T_{bio})/(t_{peak}-t_{bio})$, with pressures converted to the equivalent depth in kilometres. The range in the calculated cooling and exhumation rate arises from the range in t_{peak} from 550-520 Ma. An upper limit on the cooling and exhumation rate at Rundvågshetta is not given because the time constraints for peak metamorphism and for cooling through 300°C overlap, allowing for extremely high values. Tighter constraints on the timing of peak metamorphism are required before maximum estimates for cooling and exhumation rate can be made.

for hornblende, ~300°C for biotite and <300°C for K-feldspar (*e.g.*, MCDOUGALL and HARRISON, 1988), these results suggest cooling through the temperature interval ~500°C to <300°C at an average rate of ~9.5°C/Ma (Fig. 3).

3.6. Cape Hinode

Cape Hinode is situated on the Prince Olav Coast at 68°09′S, 42°40′E. About 20 km² of rock is exposed around a headland which rises ~200 m above sea level. This area lies between the staurolite-out and (epidote+quartz)-out isograds of HIROI *et al.* (1991).

In contrast to most of the localities discussed above, large parts of Cape Hinode consist of broken rubble or moraine, rather than fresh, glacially scoured pavements. The lithology over most of the area is dominated by monotonous, medium-grained, dark grey to purple, trondhjemitic gneiss, composed of plagioclase-quartz-hornblende-biotite. This rock shows only a weak foliation which is folded around a large-scale, tight antiform, trending north-west. To the southwest of Cape Hinode, separated from the metatrondhjemites by a few hundred metres of intervening ice sheet, are several small outcrops of psammitic and pelitic gneisses. These consist of garnet-biotite gneiss and garnet-biotite-sillimanite gneiss, and have been highly migmatised. Leucosomes generally parallel the gneissic fabric but in places are aligned along the axial planes of tight folds. In places these leucosomes coalesce to form concordant pegmatitic layers up to 1 m wide. These metasedimentary rocks appear lithologically and structurally similar to the layered gneisses studied elsewhere in the LHC. Their relationship with the trondhjemitic rocks is unclear and it is unfortunate that the contact is obscured by ice. Discordant pegmatites cross-cut both the metatrondhjemitic gneisses and the paragneisses to the southwest.

3.6.1. Samples from Cape Hinode

CH-15 (ANU no. 93-551) This sample is a pegmatite composed of coarse grained plagioclase-quartz-K-feldspar and biotite sitting within highly migmatitised garnet-biotite and garnet-sillimanite gneiss at the southernmost outcrops at Cape Hinode. Leucosomes

in the gneiss range from very thin veins, up to several centimetres wide and collect together to form the pegmatite CH-15. The pegmatite is about 2 m wide and follows the trend of the gneissic layering. This rock is therefore regarded as a consequence of partial melting in pelitic and semi-pelitic gneiss.

Biotite gives a K/Ar age of 480±5 Ma and a $^{40}Ar/^{39}Ar$ age spectrum in which 72% of the ^{39}Ar is released in 9 consecutive steps (690 to 1100°C) with an combined age of 480.7±0.5 Ma (Fig. 2), and a total fusion age of 478±1 Ma. This is indistinguishable from biotite ages from Kasumi Rock.

CH-17 (ANU no. 93-553) This sample comes from a discordant muscovite-bearing pegmatite at Cape Hinode. This is the only locality where muscovite has been found in pegmatite. Muscovite from this sample gives an age of 499±5 Ma.

CH-4 (ANU no. 93-540) This is an amphibolitic gneiss from Otome Point sitting within the surrounding trondhjemitic gneisses. Hornblende is a major constituent of this rock, together with plagioclase and minor clinopyroxene, and is aligned into a strong fabric. Hornblende gives an K/Ar age of 526±5 Ma but has not been analysed by the $^{40}Ar/^{39}Ar$ method and consequently this age remains a maximum estimate owing to the possible presence of excess radiogenic argon.

3.6.2. Discussion of ages from Cape Hinode

Of the six localities in the LHC where SHRIMP zircon dating has been done, Cape Hinode is the only one in which 500-550 Ma ages have not been found. The youngest zircon component found at Cape Hinode has an age of 1017±13 Ma (SHIRAISHI *et al.*, 1994). The dominant metatrondhjemitic lithology at Cape Hinode is also significantly different from the interlayered para- and ortho- gneiss sequences common elsewhere in the LHC. This evidence lead SHIRAISHI *et al.* (1994) to suggest that Cape Hinode represents an exotic, tectonic slice within the otherwise coherent gneisses of the LHC. However, the K/Ar ages obtained from Cape Hinode in this study are consistent with those from elsewhere in the LHC, showing no evidence of a distinct cooling history for Cape Hinode. The biotite age from a partial melt implies that the area did not finally cool below 300°C until 480±5 Ma; this is indistinguishable from biotite ages from similar rocks at Kasumi Rock. The muscovite age of 499±5 Ma, with muscovite having a closure temperature slightly higher than that of biotite (MCDOUGALL and HARRISON, 1988), shows that at Cape Hinode, discordant pegmatites intruded before the gneiss cooled below 300°C. This contrasts with the evidence from Rundvågshetta where late-stage, linear pegmatites post-date biotite ages from the gneiss sequence. At Cape Hinode the hornblende K/Ar age of 526±5 Ma combined with the biotite age of 480±5 Ma gives an average cooling rate for the temperature interval 500-300°C of ~4°C/Ma. However, the possible presence of excess argon in the hornblende (which will cause the K/Ar age to be unrealistically old) means this represents a minimum estimate for the cooling rate.

4. Discussion of Cooling History in the LHC

In order to convert the geochronological data into estimates for cooling and/or exhumation rates, it is necessary to make certain assumptions linking the age constraints with independently derived metamorphic constraints. The significance of the K/Ar and $^{40}Ar/^{39}Ar$ ages for the metamorphic history is reasonably well constrained, since the closure

temperatures of the commonly dated minerals are relatively well known from empirical observations. Thus, the K/Ar and $^{40}Ar/^{39}Ar$ mineral ages define points in the temperature versus time curves of Fig. 3. The interpretation of the zircon age data is more problematic. In contrast to K/Ar and $^{40}Ar/^{39}Ar$ ages, which represent cooling or "closure" ages, U-Pb zircon ages are generally thought to represent the crystallisation age of the zircon. The fact that inherited zircon can retain its pre-existing U-Pb signature through granulite facies metamorphism illustrates how robust this isotopic system is. However, since zircon is an accessory mineral, and *P-T* estimates are derived from equilibria between major metamorphic phases, the metamorphic significance of a zircon crystallisation age is not always clear. This is an important general problem in linking metamorphic and geochronological evidence in high-grade terrains, and is the subject of work in progress. For the purposes of constraining retrograde cooling and exhumation rates, and in the absence of compelling evidence to the contrary, we assume that the 550 to 520 Ma zircon ages of SHIRAISHI *et al.* (1994) represent the time of peak metamorphic conditions throughout the LHC. Having made this assumption, it is possible to calculate average cooling rates over the time interval from peak metamorphism until the terrain cooled below the biotite K/Ar closure temperature of ~300°C. Average cooling rates calculated and cooling curves are given for several localities in Table 3 and Fig. 3. Rundvågshetta, the locality which has experienced the highest metamorphic grade in the LHC, has also experienced the most rapid cooling.

In order to link closure temperature to depth at the time of closure, and thus to calculate exhumation rates, it is necessary to make further assumptions regarding the appropriate geotherm. The simplest scenario is to assume that a standard model geotherm for appropriate thickness crust applies during exhumation. Implicit in this assumption is that cooling is controlled by exhumation, rather than removal of a heat source. While this cannot be assumed for all high-grade terrains, there is evidence in the LHC that high grade metamorphic conditions were in fact closely followed by exhumation. This evidence comes from metamorphic reaction textures indicating decompression at near peak temperatures (KAWASAKI *et al.*, 1993), implying exhumation rates high enough for decompression to dominate over cooling at least in the immediately post-peak history. By bringing hot rocks closer to the earth's surface, such isothermal decompression must be followed by cooling towards a more stable geotherm, with the magnitude and rate of that cooling controlled by the amount of exhumation. Additional evidence for exhumation comes simply from the magnitude of cooling required for biotite closure in the K/Ar system. Metamorphic equilibria suggest that peak conditions in the LHC occurred at pressures of at least ~0.55 GPa, and up to ~1.0 GPa at Rundvågshetta. Standard model geotherms for continental crust (*e.g.*, FOWLER, 1990) require that rocks cooling through ~300°C must be at depths no greater than ~13 km, corresponding to pressure of ~0.4 GPa. Thus ~0.15–0.6 GPa of decompression (corresponding to ~4–20 km of exhumation) must have occurred between the time of peak metamorphism and the K/Ar closure ages for biotites. Elevated crustal geotherms, as may be more appropriate in actively exhuming belts such as the LHC, require exhumation to even shallower levels, making the exhumation rates calculated here minimum estimates. Following this logic, average rates of exhumation have been calculated for four localities in Table 3, once again assuming that zircon ages represent peak metamorphic conditions. Exhumation rates calculated in this way show

Rundvågshetta to have been exhumed much more rapidly than Austhovde or Kasumi Rock. Exhumation rates for Austhovde and Kasumi Rock are relatively low in comparison to a compilation of exhumation rates from several orogenic areas given by DODSON and MCCLELLAND-BROWN (1985). The higher exhumation rate for Rundvågshetta of >1.0 mm/yr falls within the range of orogenic values given in DODSON and MCCLELLAND-BROWN (1985), and is comparable with estimates of >3 mm/yr for the Tauern Window (CLIFF *et al.*, 1985) and ~5 mm/yr for Nanga Parbat (ZEITLER *et al.*, 1993). GUILLOT *et al.* (1995) suggest that exhumation rates >1 mm/yr require tectonic unroofing by normal faulting. It should be emphasised that both the cooling and exhumation rates calculated here are *average* rates over periods of several tens of million years, and that, as mentioned above, the exhumation rates are minimum estimates. Actual values of cooling and exhumation rate are likely to have varied in a complex manner during a retrograde *P-T* history involving initial isothermal decompression and subsequent cooling. Thus the relatively high average exhumation rate for Rundvågshetta may well be indicative of tectonic unroofing for at least part of the post-peak history of this area. Cooling and exhumation rates for Cape Hinode have not been calculated in Table 3 because there is considerable uncertainty regarding the origin of these rocks relative to other parts of the LHC. If Cape Hinode does in fact represent an exotic, tectonic slice, as has been suggested by SHIRAISHI *et al.* (1994), the results of this study suggest that it must have been tectonically emplaced into the LHC prior to ~520 Ma and subsequently experienced a thermal history in common with other parts of the LHC.

5. Conclusions

Dr. David ELLIS is thanked for suggesting this project, and was instrumental in arranging field work for G.F. Best estimates for timing of peak metamorphism and orogenesis come from SHRIMP zircon ages ranging from 520 to 550 Ma (SHIRAISHI *et al.*, 1994, and work in progress). K/Ar and $^{40}Ar/^{39}Ar$ results show that regional cooling to $<$ 300°C had taken place throughout the LHC by ~450 Ma. The data presented here suggest that, despite an apparently similar style of *P-T-t* history across the LHC (HIROI *et al.*, 1991), the timing and rate of retrograde *P-T* evolution varied within the terrain, with the region of highest metamorphic grade experiencing more rapid exhumation and cooling than lower grade areas.

Acknowledgments

The Japanese Antarctic Research Expeditions (JARE) provided logistical support for G.F. for the 1992-93 and 1993-94 field seasons. All members of JARE-34 and -35 and the crew of icebreaker SHIRASE are thanked for making the field seasons such a memorable experience. The Japan Polar Research Association provided financial support for G.F. to visit NIPR and present this work at the 14th Symposium on Antarctic Geosciencesin 1994. Dr. Y. MOTOYOSHI, M. ISHIKAWA, Prof. K. SHIRAISHI and Prof. Y. HIROI are thanked for numerous discussions and for their hospitality. Robyn MAIER and Terry SPELL provided excellent support during the laboratory analyses. The comments of two anonymous reviewers are appreciated.

References

CLIFF, R.A., DROOP, G.T.R. and REX, D.C. (1985): Alpine metamorphism in the south-east Tauern Window, Austria: 2. Rates of heating, cooling and uplift. J. Metamorph. Geol., **3**, 403–415.

DALRYMPLE, G.B. and LANPHERE, M.A. (1969): Potassium-Argon Dating. San Francisco, Freeman.

DALZIEL, I.W.D. (1991): Pacific margins of Laurentia and East Antarctica–Australia as a conjugate rift pair: Evidence and implications for an Eocambrian supercontinent. Geology, **19**, 598–601.

DODSON, M.H. and MCCLELLAND-BROWN, E. (1985): Isotopic and palaeomagnetic evidence for rates of cooling, uplift and erosion. The Geochronology of the Geological Record, ed. by N.J. SNELLING. London, Spec. Publ. Geol. Soc.

FOWLER, C.M.R. (1990): The Solid Earth: An Introduction to Global Geophysics. Cambridge, Cambridge University Press.

GUILLOT, S., LEFORT, P., PECHER, A., BARMAN, M.R. and APRAHAMIAN, J. (1995): Contact metamorphism and depth of emplacement of the Manaslu granite (central Nepal). Implications for Himalayan orogenesis. Tectonophysics, **241**, 99–119.

HARRISON, T.M., DUNCAN, I. and MCDOUGALL, I. (1985): Diffusion of ^{40}Ar in biotite: Temperature, pressure and compositional effects. Geochim. Cosmochim. Acta, **49**, 2461–2468.

HIROI, Y., SHIRAISHI, K. and MOTOYOSHI, Y. (1991): Late Proterozoic paired metamorphic complexes in East Antarctica, with special reference to the tectonic significance of ultramafic rocks. Geological Evolution of Antarctica, ed. by M.R.A. THOMSON *et al.* Cambridge, Cambridge University Press, 83–87.

HÖLZL, S., HOFMANN, A.W., TODT, W. and KÖHLER, H. (1994): U-Pb geochronology of the Sri Lankan basement. Precambrian Res., **66**, 123–149.

ISHIKAWA, M., MOTOYOSHI, Y., FRASER, G.L. and KAWASAKI, T. (1994): Structural Evolution of Rundvågshetta region, Lützow-Holm Bay, East Antarctica. Proc. NIPR Symp. Antarct. Geosci., **7**, 69–89.

KANEOKA, I., OZIMA, M., AYUKAWA, M. and NAGATA, T. (1968): K/Ar ages and paleomagnetic studies on rocks from the east coast of Lützow-Holm Bay, Antarctica. Nankyoku Shiryô (Antarct. Rec.) **31**, 12–20.

KAWASAKI, T., ISHIKAWA, M. and MOTOYOSHI, Y. (1993): Preliminary report on cordierite bearing assemblages from Rundvågshetta, Lützow-Holm Bay, East Antarctica: Evidence for a decompressional *P-T* path ? Proc. NIPR Symp. Antarct. Geosci., **6**, 47–56.

KRÖNER, A. and WILLIAMS, I.S. (1993): Age of metamorphism in the high-grade rocks of Sri Lanka. J. Geol., **101**, 513–521.

LOVERA, O.M., RICHTER, F.M. and HARRISON, T.M. (1989): $^{40}Ar/^{39}Ar$ geothermometry for slowly cooled samples having a distribution of diffusion domain sizes. J. Geophys. Res., **94**, 17917–17936.

MCDOUGALL, I. and HARRISON, T.M. (1988): Geochronology and Thermochronology by the $^{40}Ar/^{39}Ar$ Method. New York, Oxford University Press.

MOTOYOSHI, Y. (1986): Prograde and progressive metamorphism of the granulite-facies Lützow-Holm Bay region, East Antarctica. D. Sc. thesis, Hokkaido University, 238 p.

MOTOYOSHI, Y. and SHIRAISHI, K. (1985): Petrography and geothermometry-geobarometry of Botnnuten, East Antarctica. Mem. Natl Inst. Polar Res., Spec. Issue, **37**, 127–146.

MOTOYOSHI, Y., ISHIKAWA, M., FRASER, G. and KAWASAKI, T. (1993): Metamorphism of the Lützow-Holm Complex revisited (abstract). The 14th Symposium on Antarctic Geoscieces Programme and Abstracts. Tokyo, Natl Inst. Polar Res., 62–63.

PAQUETTE, J-L., NEDELEC, A., MOINE, B. and RAKOTONDRAZAFY, M. (1994): U-Pb, single zircon Pb-evaporation, and Sm-Nd isotopic study of a granulite domain in SE Madagascar. J. Geol., **102**, 523–538.

SHIBATA, K., YANAI, K. and SHIRAISHI, K. (1985): Rb-Sr mineral isochron ages of metamorphic rocks around Syowa Station and from the Yamato Mountains, East Antarctica. Mem. Natl Inst. Polar Res., Spec. Issue, **37**, 164–171.

SHIRAISHI, K., ELLIS, D.J., HIROI, Y., FANNING, C.M., MOTOYOSHI, Y. and NAKAI, Y. (1994): Cambrian

orogenic belt in East Antarctica and Sri Lanka: Implications for Gondwana assembly. J. Geol., **102**, 47–65.

TAKIGAMI, Y., FUNAKI, M. and TOKIEDA, K. (1992): $^{40}Ar/^{39}Ar$ geochronological studies on some paleomagnetic samples of East Antarctica. Recent Progress in Antarctic Earth Science, ed. by Y. YOSHIDA *et al.*, Tokyo, Terra Sci. Publ., 61–66.

YANAI, K. and UEDA, Y. (1974): Absolute ages and geological investigations on the rocks in the area around Syowa Station, East Antarctica. Nankyoku Shiryô (Antarct. Rec.), **48**, 70–81 (in Japanese with English abstract).

ZEITLER, P.K., CHAMBERLAIN, C.P. and SMITH, H.A. (1993): Synchronous anatexis, metamorphism, and rapid denudation at Nanga Parbat (Pakistan Himalaya). Geology, **21**, 347–350.

(Received March 29, 1995; Revised manuscript received June 9, 1995)